


## MATERIALS SCIENCE

# A partially fluorinated ligand for two super-hydrophobic porous coordination polymers with classic structures and increased porosities

Chao Wang, Dong-Dong Zhou, You-Wei Gan, Xue-Wen Zhang, Zi-Ming Ye and Jie-Peng Zhang \*

## ABSTRACT

3-Ethyl-5-trifluoromethyl-1,2,4-triazole is synthesized by a one-pot reaction. Using this asymmetric triazole ligand bearing one trifluoromethyl and one ethyl as side groups, we construct two new porous coordination polymers, MAF-9 and MAF-2F, being isostructural with the classic hydrophobic and flexible materials, FMOF-1 and MAF-2, based on symmetric triazole ligands bearing two trifluoromethyl groups or two ethyl groups, respectively. MAF-9 and MAF-2F can adsorb large amounts of organic solvents but completely exclude water, showing superhydrophobicity with water contact angles of  $152^\circ$  in between those of FMOF-1 and MAF-2. MAF-9 exhibits very large  $N_2$ -induced breathing and colossal positive and negative thermal expansions like FMOF-1, but the lower molecular weight and smaller volume of MAF-9 give 16% and 4% higher gravimetric and volumetric  $N_2$  uptakes, respectively. In contrast, MAF-2F is quite rigid and does not show the inversed temperature-dependent  $N_2$  adsorption and large guest-induced expansion like MAF-2. Further, despite the higher molecular weight and larger volume, MAF-2F possesses 6% and 25% higher gravimetric and volumetric  $CO_2$  uptakes, respectively. These results can be explained by the different pore sizes and side group arrangements in the two classic framework prototypes, which demonstrate the delicate roles of ligand side groups in controlling porosity, surface characteristic and flexibility.

**Keywords:** porous coordination polymers, metal-organic frameworks, super-hydrophobicity, flexibility

## INTRODUCTION

As a new type of adsorbent showing high structural regularity and extremely rich structural diversity, porous coordination polymers (PCPs) or metal-organic frameworks (MOFs) have attracted great attention for achieving extraordinary properties [1–4]. PCPs can have not only much higher flexibility [5–12], but also much higher hydrophobicity than other types of adsorbents [13–34]. Introducing hydrophobic side groups on the organic ligand is the main strategy for synthesizing/designing hydrophobic PCPs [20–33]. Due to the extremely high electronegativity of fluorine, fluorinated organic compounds usually have high hydrophobicity [20–31]. PCPs constructed by perfluorinated organic ligands are of particular interest, but reported

examples are very rare because fluorinated ligands are difficult to synthesize [23–30].

[Ag(bftz)] (FMOF-1, Hbftz = 3,5-bis(trifluoromethyl)-1,2,4-triazole) is a classic PCP constructed by a perfluorinated organic ligand [27], which can readily adsorb carbon dioxide and various hydrocarbons and completely exclude water [22,23]. FMOF-1 is also noteworthy for its remarkably large  $N_2$ -induced framework breathing, colossal positive/negative thermal expansion, and low dielectric constant [28,35]. Nevertheless, the synthesis of the perfluorinated organic ligand Hbftz requires six-step reactions, and the synthesis of FMOF-1 also requires several reaction-evaporation-recrystallization steps using several organic solvents [27,36], which impede the study/application of this classic PCP.

MOE Key Laboratory of Bioinorganic and Synthetic Chemistry, School of Chemistry, Sun Yat-Sen University, Guangzhou 510275, China

\*Corresponding author. E-mail: zhangjp7@mail.sysu.edu.cn

Received 27 February 2020;  
Revised 20 April 2020; Accepted 26 April 2020

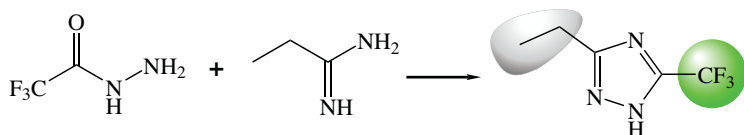


**Figure 1.** One-step synthesis of Hfetz. The sizes and shapes of the side groups are highlighted.

Based on the more common alkyl groups, we have designed and synthesized a series of hydrophobic porous metal azolate frameworks (MAFs) with high stability and interesting properties [37]. For example, [Cu(detz)] (MAF-2, Hdetz = 3,5-diethyl-1,2,4-triazole), as a rare Cu(I)-based PCP showing high stability toward water and oxygen, can be used to separate organic solvents from water and sense oxygen in air and water [38,39]. Besides multimode distortion of the Cu(I)-triazolate scaffold in response to different organic molecules, MAF-2 also exhibits aperture dynamism originated from the flexible ethyl groups, which give inverted temperature-dependence of  $N_2$  adsorption [38].

Recently, we found that partially fluorinated azoles are relatively easy to synthesize and can be used to construct highly hydrophobic and stable PCPs [20,21]. For example, 3-methyl-5-trifluoromethyl-1,2,4-triazole can be synthesized from trifluoroacetohydrazide and acetamidine hydrochloride by a one-pot reaction [40]. Here, we report two new superhydrophobic PCPs, namely [Ag(fetz)] (MAF-9) and [Cu(fetz)] (MAF-2F), being isostructural with the classic materials FMOF-1 and MAF-2, respectively, by using an easily synthesized, partially fluorinated ligand 3-ethyl-5-trifluoromethyl-1,2,4-triazole (Hfetz).

## RESULTS AND DISCUSSION

### Synthesis

The ligand Hfetz can be synthesized in high yield by a one-pot reaction between trifluoroacetohydrazide and propionamidine hydrochloride (Fig. 1; Figs S1 and S2) [40]. Hfetz can dissolve in  $CHCl_3$ , benzene, toluene, xylene, ethanol and methanol, but is insoluble in water. Room temperature diffusion of the methanol solution of Hfetz and aqueous solution of  $AgNO_3$  with toluene as a buffer layer yielded colorless, block-shaped single crystals of MAF-9. Solvothermal reaction of  $Cu(NO_3)_2$  and Hfetz in water/toluene mixed solvent yielded single crystals of MAF-2F [37]. Microcrystalline MAF-9 and MAF-2F can be synthesized facilely by fast mixing of the toluene solution of Hfetz and the aqueous solution of  $AgNO_3$  at room temperature (Fig. S3), or by re-

fluxing  $Cu_2O$  nanocrystals and Hfetz in ethanol under oxygen-free conditions (Fig. S4).

Various Ag(I) 1,2,4-triazolate structures have been reported [41–45], but only one (3,5-diphenyl-1,2,4-triazolate, nonporous because of the bulky phenyl groups) is isostructural or isorecticular with FMOF-1 [41]. Ag(I) 3,5-diethyl-1,2,4-triazolate crystallizes as complicated three-dimensional (3D) coordination frameworks with inaccessible pores [42]. [Cu(dptz)] (Hdptz = 3,5-dipropyl-1,2,4-triazole) [37] and [Ag(diptz)]· $C_6H_6$  (Hdiptz = 3,5-diisopropyl-1,2,4-triazole) [42] possess the **nbo-a** typology of MAF-2, but they crystallize in the expanded cubic form and have negligible or no porosity because of the large side groups. We have also investigated the self-assembly of 3-methyl-5-trifluoromethyl-1,2,4-triazole and copper salts, but failed to obtain binary coordination polymers so far [20]. These results demonstrated the important role of uncoordinated side groups in determining the supramolecular structures [37].

### Structure

Single-crystal X-ray diffraction (SCXRD) revealed that MAF-9 and MAF-2F are isostructural with FMOF-1 (tetragonal *I-42d*) and MAF-2 (trigonal *R-3*), respectively (Table S1 and Figs S5 and S6). MAF-9 exhibits a unit-cell volume 1.9% smaller than that of FMOF-1, because the Ag–N bond lengths are ca. 0.1 Å shorter in the former structure (Table S2), which can be attributed to the electron withdrawing and donating nature of the  $-CF_3$  and  $-C_2H_5$  groups which weakens and strengthens the coordination bond, respectively. The void ratio of MAF-9 (41.0%) is smaller than that of FMOF-1 (44.4%), but the crystallographic pore volume of MAF-9 is slightly larger than that of FMOF-1 (Table S3), because  $-C_2H_5$  is larger but lighter than  $-CF_3$ .

The unit-cell volume of MAF-2F is 3.0% larger than that of MAF-2, although the Cu–N bonds are only ca. 0.01 Å longer in the former structure (Tables S1 and S4). The variation of the unit-cell volume is mainly related to the conformation of the **nbo-a** network. The interplanar angles of the adjacent square nodes in MAF-2 and MAF-2F are 79.9° and 84.4°, respectively (Fig. S7) [38]. An interplanar angle closer to 90° means the network is closer to the ideal cubic symmetry with the largest volume. The relatively large interplanar angle of MAF-2F indicates that the  $-CF_3$  groups in this structure prototype have larger steric hindrance effect than  $-C_2H_5$  groups. Although  $-C_2H_5$  is larger than  $-CF_3$ , this can happen when these side groups

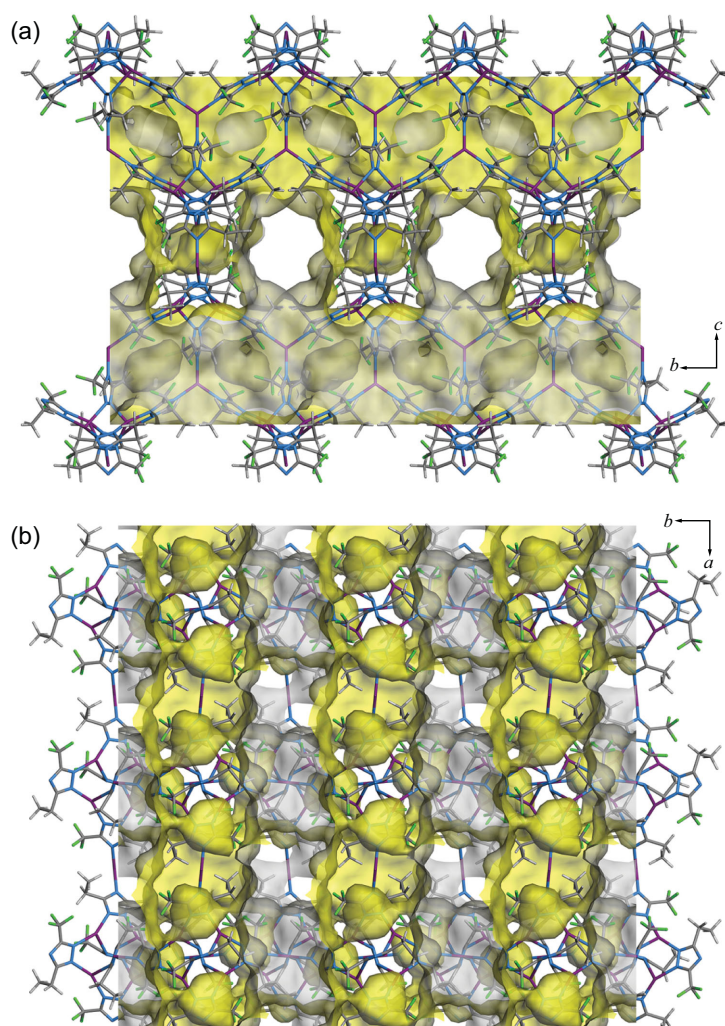


**Figure 2.** Framework and pore structures of MAF-9 viewing along (a) the *a*-axis and (b) the *c*-axis. The asymmetric  $\text{fetz}^-$  ligand is two-fold disordered in the crystal structure. Shown here is an average structure.

locate closely, since  $-\text{CF}_3$  is larger than  $-\text{CH}_2-$ . The void ratio of MAF-2F (38.3%) is much larger than that of MAF-2 (31.3%), but the difference of the crystallographic pore volume is small (Table S5).

Similar to FMOF-1, MAF-9 possesses a 3D intersecting channel system with the 3-connected (10,3)-*b* (*ths*) topology (38.0%), and some very small, discrete cavities (3.0%) separated from the main 3D channel by the side groups (Fig. 2). Because some of the  $-\text{CF}_3$  groups are replaced by  $-\text{C}_2\text{H}_5$  groups, some discrete cavities may become accessible from the 3D channel (Figs S8–S10). The channel apertures of MAF-9 and FMOF-1 viewing along the *a*- and *b*-axes are ellipsoidal ( $4.0\text{--}5.9 \times 6.6 \text{ \AA}^2$ ) and rectangular ( $5.8 \times 7.9 \text{ \AA}^2$ ), respectively, because the long and flexible ethyl groups locate at the aperture corners.

Just like MAF-2 possessing a distorted **nbo-a** coordination network and a distorted **bcu** pore system,

there are large cavities and two types of apertures in MAF-2F. Along the *c*-axis, the aperture with an effective diameter of  $2.5 \text{ \AA}$  is defined by six surrounding  $-\text{CF}_3$  groups (Fig. 3a), which is much larger than that of MAF-2 ( $1.1 \text{ \AA}$ ) defined by six  $-\text{C}_2\text{H}_5$  groups (Fig. 3b). Another type of aperture (not pointing to special crystallographic direction) is surrounded by four  $-\text{C}_2\text{H}_5$  groups and two  $-\text{CF}_3$  groups with negligible effective size (Fig. 3c), being similar with that of MAF-2 (Fig. 3d). In other words, in the static point of view, the pore systems of MAF-2 and MAF-2F can be regarded as 0D and 1D, respectively, for a guest molecule (e.g.  $\text{H}_2$ ) with a diameter smaller than  $2.5 \text{ \AA}$  (Fig. 3).

### Stability and hydrophobicity

Thermogravimetry showed long plateaus from room temperature to  $280^\circ\text{C}$  for MAF-9 and MAF-2F, meaning that the as-synthesized samples contained no guest molecules (Figs S11 and S12), exemplifying their hydrophobic pores. Compacted samples of microcrystalline MAF-9 and MAF-2F both show water contact angles of  $152^\circ$  (Fig. 4) and glide angles of less than  $4^\circ$  (Figs S13 and S14), meaning that their crystal surfaces are superhydrophobic, which have only been observed in a few PCPs [13–16,21–24,33,34]. The water contact angle of FMOF-1 was reported as  $158^\circ$  [22], while that of MAF-2 was measured as  $140^\circ$  (Fig. S15), which exemplifies the higher hydrophobicity of  $-\text{CF}_3$  compared with  $-\text{C}_2\text{H}_5$ , and the ability of tuning hydrophobicity by mixing these functional groups.

MAF-9 can keep its powder X-ray diffraction (PXRD) pattern and color unchanged in water and/or under sunlight at room temperature for at least one year (Fig. S3). MAF-2F can also maintain its PXRD pattern and color in water and/or humid air at room temperature for at least three months (Fig. S4). For comparison, FMOF-1 was reported to be stable after being exposed to saturated water vapor for 70 days at room temperature [28]. MAF-2 was reported to be able to keep its PXRD pattern unchanged in water for at least one year, but turned light green in humid conditions after several days due to the oxidation of the crystal surface [39].

### Gas adsorption and flexibility

MAF-9 shows an apparent type-I  $\text{N}_2$  adsorption isotherm at  $77 \text{ K}$ , but there is an additional step around  $P/P_0 = 0.001$  (Fig. 5a and Fig. S16), which is very similar with that of FMOF-1 [27]. The saturated  $\text{N}_2$  uptake and corresponding experimental pore volume of MAF-9 are 16% larger than those of FMOF-1, consistent with the difference of their

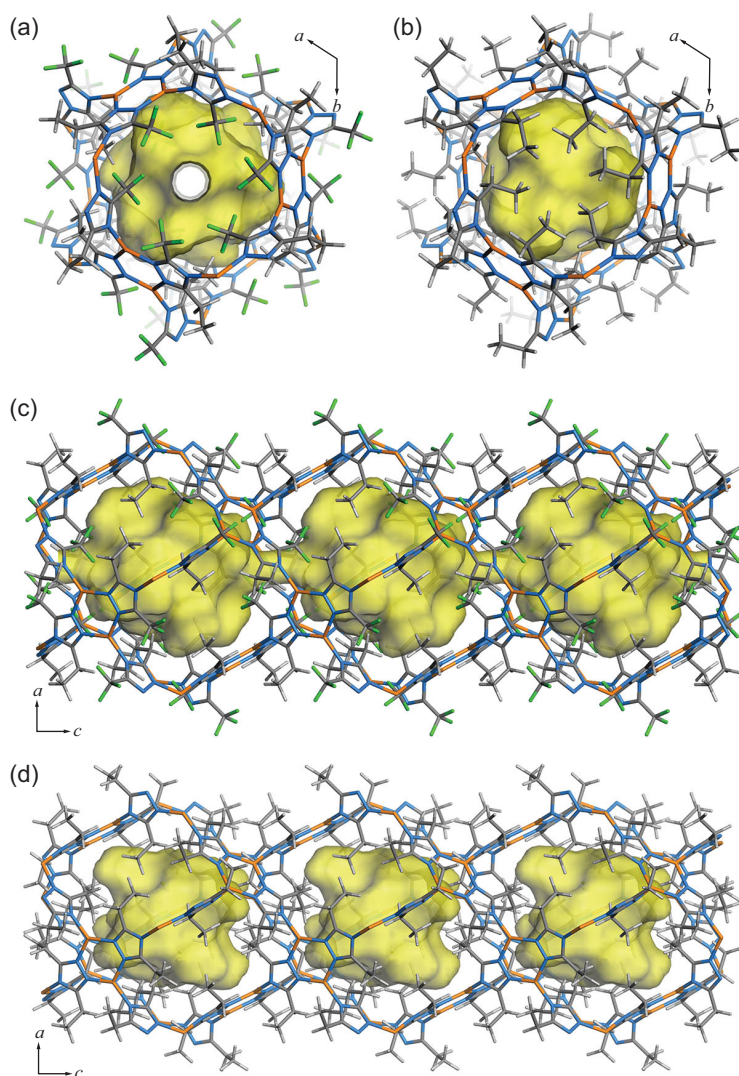


**Figure 3.** Framework and pore structures of (a, c) MAF-2F and (b, d) MAF-2 viewing along the *c*-axis (a, b) and the *a*-axis (c, d).

molecular weights (Table S3). Actually, the two isostructural PCPs show similar or the same host-guest stoichiometries of  $N_2/Ag \approx 1.3$  and  $N_2/Ag = 3.0$  at the two isotherm steps (Fig. S16). The very similar  $N_2$  adsorption isotherms imply that they share the same adsorption mechanism, which has been elucidated by *in situ* SCXRD for FMOF-1, i.e. the host first contracts ( $-8.6\%$ ) by adsorbing  $N_2$  only in the 3D channel, and then expands to a state larger than the guest-free state ( $3.4\%$ ) by additional adsorption of  $N_2$  not only in the 3D channel but also in the 0D cavities [35]. The higher host-guest stoichiometry of MAF-9 at the first isotherm step might be attributed to the existence of some accessible 0D cavities (Figs S8–S10).

Considering that guest-free FMOF-1 is also highly flexible toward temperature, we measured

the SCXRD structure of MAF-9 at low temperature (Table S1), giving very large positive and negative thermal expansion coefficients ( $\alpha_a = 2.38 \times 10^{-4} \text{ K}^{-1}$ ,  $\alpha_c = -2.06 \times 10^{-4} \text{ K}^{-1}$  and  $\beta = 2.68 \times 10^{-4} \text{ K}^{-1}$ ), being similar with those reported for FMOF-1 under vacuum ( $\alpha_a = 2.3 \times 10^{-4} \text{ K}^{-1}$ ,  $\alpha_c = -1.7 \times 10^{-4} \text{ K}^{-1}$  and  $\beta = 3.0 \times 10^{-4} \text{ K}^{-1}$ ) [35]. Note that, because MAF-9 has a smaller unit-cell volume, its volumetric porosity is also higher than that of FMOF-1 (Table S3).

MAF-2F exhibits a typical type-I  $N_2$  adsorption isotherm at 77 K (Fig. 6a; Figs S17 and S18). The pore volume calculated from the  $N_2$  isotherm fits well with crystallographic value (Table S5). In contrast, MAF-2 cannot adsorb  $N_2$  at 77 K, because the static sizes of the apertures are too small and the  $-C_2H_5$  groups are not dynamic enough at such a low temperature [38]. In this context, the relatively large aperture of MAF-2F along the *c*-axis and the dynamism of  $-CF_3$  groups should be responsible for its  $N_2$  adsorption at 77 K, since the static size of the aperture is just slightly smaller than the guest molecule. At 195 K, MAF-2F shows a type-I  $CO_2$  isotherm with a pore volume slightly smaller than the crystallographic value (Table S5). Regardless of its higher molecular weight, the gravimetric saturated  $CO_2$  uptake of MAF-2F is 6% higher than that of MAF-2 [46]. In the volumetric point of view, the saturated  $CO_2$  uptake of MAF-2F is 25% higher than that of MAF-2. More straightforwardly, the host-guest stoichiometry of MAF-2F ( $1.39 \text{ CO}_2/\text{Cu}$ ) is significantly larger than that of MAF-2 ( $1.08 \text{ CO}_2/\text{Cu}$ ), meaning that the  $CO_2$  molecules arrange differently in the two isostructural PCPs. The different  $CO_2$  adsorption mechanisms of MAF-2F and MAF-2 can be visualized by Grand Canonical Monte Carlo (GCMC) simulations (Figs S19 and S20).

### Vapor adsorption and hydrophobicity/flexibility

MAF-9 shows type-V methanol, ethanol and benzene vapor adsorption isotherms, meaning that the host-guest interactions are weaker than the guest-guest interactions (Fig. 5b and Fig. S21) [47]. The initial isotherm slope follows benzene > ethanol > methanol, consistent with the trends of guest hydrophobicity and molecular weight, which can be explained by the fact that a larger molecule generally has stronger interaction with the host framework. The benzene adsorption capacity of MAF-9 ( $2.36 \text{ mmol g}^{-1}$ ) is 6% higher than that of FMOF-1 ( $2.23 \text{ mmol g}^{-1}$ ) [23]. Thermogravimetry showed that MAF-9 can also adsorb considerable

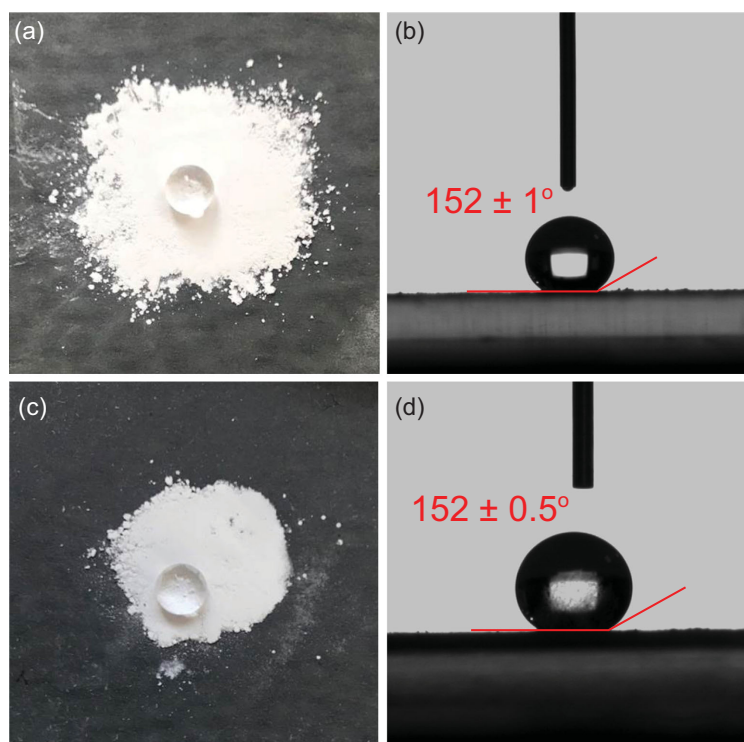


**Figure 4.** Typical photographs for water contact angle tests for (a, b) MAF-9 and (c, d) MAF-2F.

amounts of large aromatic molecules such as *p*-xylene, *m*-xylene, *o*-xylene, cyclohexane and mesitylene (Fig. S11). By contrast, MAF-9 completely excludes water ( $0.07 \text{ mmol g}^{-1}$  at  $P/P_0 = 0.99$ ), highlighting its high hydrophobicity (Fig. 5b). PXRD showed that the unit-cell parameters of MAF-9 in water are almost the same as those in air (Figs S22–S33 and Table S6), consistent with its high hydrophobicity. On the other hand, in organic solvents, the unit-cell volume of MAF-9 can increase up to 6.1% (*o*-xylene) or decrease up to 0.7% (ethanol); the *a*-axis can increase up to 5.3% (*o*-xylene) or decrease up to 1.5% (ethanol); and the *c*-axis can increase up to 2.2% (ethanol) or decrease up to 4.8% (mesitylene) (Table S6).

MAF-2F also shows type-V adsorption isotherms for methanol, ethanol and benzene, and completely excludes water ( $0.06 \text{ mmol g}^{-1}$  at  $P/P_0 = 0.99$ ), being similar with MAF-9, FMOF-1 and MAF-2 (Fig. 6b and Fig. S34) [23,38]. Using the saturated methanol, ethanol and benzene uptakes of 4.8, 4.4 and  $2.1 \text{ mmol g}^{-1}$ , the host-guest stoichiometries can be calculated as 1.09, 1.00 and 0.48 guest/Cu, respectively, just the same as those of MAF-2, meaning that these relatively large guest molecules have the same and ordered arrangements in the two analogues [38].

PXRD showed that MAF-2F shows negligible volume change ( $\Delta V < 0.5\%$ ) after adsorbing water,

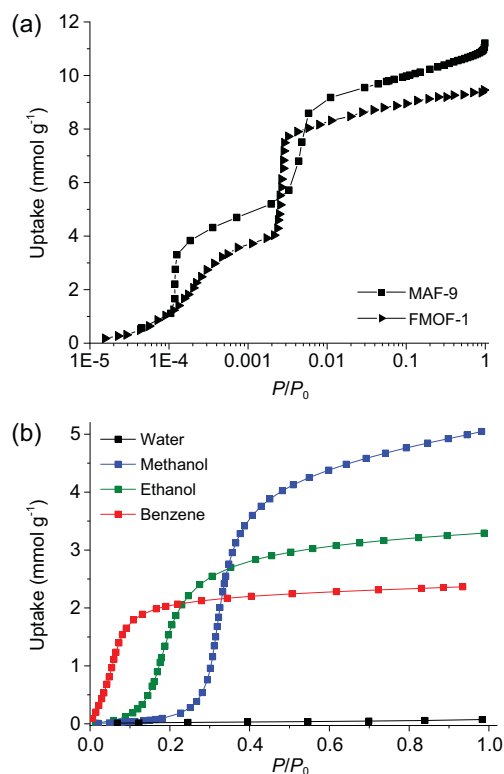


**Figure 5.** (a) 77-K  $\text{N}_2$  adsorption isotherms of MAF-9 and FMOF-1 and (b) 298-K water, methanol, ethanol and benzene vapor adsorption isotherms of MAF-9.

methanol, ethanol or benzene (Figs S35–S40 and Table S7). In contrast, MAF-2 expands 4.4% and transforms from the trigonal conformation to the cubic conformation after adsorbing benzene [38]. This indicates that MAF-2F is much less flexible than MAF-2. As exemplified by the larger interplanar angle of MAF-2F, the six  $-\text{CF}_3$  groups gathering at the apertures running along the *c*-axis endure stronger steric hindrance with each other, which can prevent the Cu(I) triazolate framework from guest-induced distortion. It should be noted that, even if the Cu(I) triazolate framework of MAF-2F expands to adopt the cubic symmetry, the presence of two types of apertures (surrounded by different numbers of  $-\text{CF}_3$  and  $-\text{C}_2\text{H}_5$  groups) in a 1:3 ratio gives the whole framework a trigonal symmetry.

## CONCLUSION

By mixing the trifluoromethyl and ethyl groups in the triazolate ligand, we obtained two new PCPs being isostructural with the classic hydrophobic and flexible PCPs based on symmetric triazole ligands either fully fluorinated or non-fluorinated. The new PCPs exhibit superhydrophobicity in between the fully-fluorinated and non-fluorinated PCPs, but the

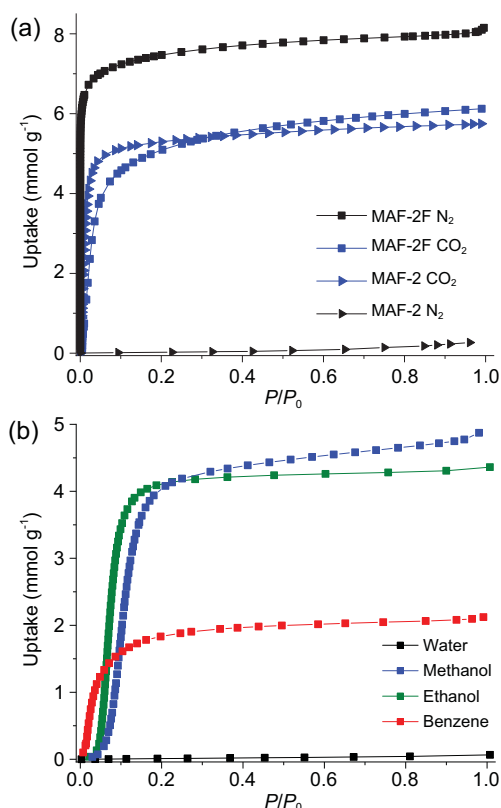


**Figure 6.** (a) 77-K N<sub>2</sub> and 195-K CO<sub>2</sub> adsorption isotherms of MAF-2F and MAF-2 and (b) 298-K water, methanol, ethanol and benzene vapor adsorption isotherms of MAF-2F.

new ligand and new PCPs are much easier to synthesize. Interestingly, regardless of changing the trifluoromethyl group to ethyl group or changing the ethyl group to trifluoromethyl group, the new PCPs show higher gas adsorption capacities, which highlights the important role of trivial modification of the size, length and thickness of ligand side groups in PCPs with small pore sizes.

## METHODS

### Materials and measurements

All reagents and solvents were commercially available and used as received without further purification. Elemental analyses (EA) were performed with a Vario El elemental analyzer. Thermogravimetry analyses were performed using a TA Q50 instrument with a heating rate of 10.0°C/min under nitrogen. Water contact angles and slide angles were measured using the KRUSS DSA100 contact angle meter using compressed powders. Nuclear magnetic resonance spectrum was measured on an AVANCE III 400 MHz spectrometer. Mass spectrum was obtained by LTQ Orbitrap Elite LC/MS (ESI) equipment with MeOH as the mobile phase.

### Synthesis of Hfetz

The synthesis method reported for Hfetz was used [40]. A mixture of ethyl trifluoroacetate (7.1 g, 50 mmol), hydrazine monohydrate (2.0 g, 50 mmol) and tetrahydrofuran (250 mL) was stirred for 1 h at reflux temperature and then cooled to room temperature. After the addition of propionamide hydrochloride (6.0 g, 55 mmol) and NaOH (2.2 g, 55 mmol), the resultant mixture was stirred for another 3 h at reflux temperature. The mixture was quenched with a cold saturated NaHCO<sub>3</sub> solution (2.5 L) and extracted with ethyl acetate (500 mL × 3). The extracts were dried with Na<sub>2</sub>SO<sub>4</sub>, filtered, and concentrated under vacuum. The residue was sublimated to give white solid (7.26 g, 88% yield): *R<sub>f</sub>* 0.55 (hexane/ethyl acetate 4:1); m.p. 130.5–131.2°C; <sup>1</sup>H NMR (400 MHz, CD<sub>3</sub>OD) δ 2.86 (q, *J* = 7.7 Hz, 2H), 1.36 (t, *J* = 7.7 Hz, 3H); ESI-MS *m/z* Calcd. for C<sub>5</sub>F<sub>3</sub>H<sub>5</sub>N<sub>3</sub><sup>-</sup> [M-H]<sup>-</sup>: 164.04, found: 164.12. EA calcd for C<sub>5</sub>F<sub>3</sub>H<sub>6</sub>N<sub>3</sub> (%): C, 36.37; N, 25.45; H, 3.66. Found. C, 36.90; N, 25.52; H, 3.62.

### Synthesis of [Ag(fetz)] (MAF-9)

Single crystals: toluene (2.5 mL) and a solution of Hfetz (0.0136 g, 0.08 mmol) in methanol (2.0 mL) were sequentially layered onto a solution of AgNO<sub>3</sub> (0.0132 g, 0.08 mmol) in water (2.0 mL). After about two weeks, colorless crystals were collected for single-crystal X-ray diffraction analyses. Microcrystalline powders: a solution of Hfetz (0.165 g, 1 mmol) in toluene (20 mL) was poured into an aqueous solution (20 mL) of AgNO<sub>3</sub> (0.170 g, 1 mmol). After the suspension was stirred for 2 h at room temperature, the white crystalline powder was filtered and washed by methanol (40 mL) three times, and then dried in air for 2 h (0.177 g, 65% yield). EA calcd (%) for AgC<sub>5</sub>F<sub>3</sub>H<sub>5</sub>N<sub>3</sub>: C 22.08, N 15.45, H 1.85; found: C 22.34, N 15.26, H 1.77.

### Synthesis of [Cu(fetz)] (MAF-2F)

Single crystals: a solution of Cu(NO<sub>3</sub>)<sub>2</sub> · 3H<sub>2</sub>O (0.5 mmol, 120.8 mg) in water (3 mL) and a solution of Hfetz (0.5 mmol, 0.0825 g) in toluene (3 mL) were mixed and sealed in a 15-mL Teflon-lined reactor, heated at 160°C for 72 h, and then slowly cooled to room temperature to give colorless crystals. Microcrystalline powders: a solution of Hfetz (0.165 g, 1 mmol) in ethanol (10 mL) was added into a suspension of Cu<sub>2</sub>O nanoparticle (0.5 mmol) in ethanol (10 mL). N<sub>2</sub> was bubbled into the mixture for 2 min to evacuate O<sub>2</sub>. The

solution was sealed in a glass bottle, refluxed for 30 min, and then slowly cooled to room temperature. The resultant white crystalline powders were filtrated, washed with ethanol three times, and then dried in air for 2 h (0.218 g, 96% yield). EA calcd(%) for  $C_5CuF_3H_5N_3$ : C 26.38, N 18.46, H 2.21; found: C 26.81, N 18.40, H 2.37.

## Sorption measurements

Gas sorption isotherms of FMOF-1 and MAF-2 were adopted from the literature [27,46]. Gas and vapor sorption isotherms of MAF-9 and MAF-2F were measured with automatic volumetric adsorption apparatuses (ASAP 2020M or BELSORP-max). The measurement temperature was controlled by a liquid-nitrogen bath (77 K), a dry ice-acetone bath (195 K) or a water bath (298 K). Before the sorption experiments, the sample was treated in high vacuum for 2 h at 383 K. Experimental pore volume was calculated based on the saturated gas uptake (read at  $P/P_0 = 0.95$ ), using the liquid  $N_2$  density of  $0.804 \text{ g cm}^{-3}$  or liquid  $CO_2$  density of  $1.104 \text{ g cm}^{-3}$ . Volumetric uptake was converted from the gravimetric uptake using the crystal density, supposing that the material did not change volume after adsorption, which was basically valid for MAF-2/MAF-2F during  $N_2/CO_2$  adsorption. FMOF-1/MAF-9 breathed significantly during  $N_2$  adsorption with very similar amplitudes, so that the absolute volumetric uptakes have relatively large errors, but they can be compared with each other.

## X-ray crystallography

Single-crystal X-ray diffraction intensities of MAF-9, MAF-2F and MAF-2 were collected on a Pilatus XtaLAB P300DS or a Rigaku Oxford SuperNova single-crystal diffractometer by using graphite monochromated  $Cu-K\alpha$  radiation. Absorption corrections were applied by using the multi-scan program REQAB or CrysAlisPro. The structures were solved by the direct method and refined by the full-matrix least-squares method on  $F^2$  with SHELXTL-2014 package. Anisotropic thermal parameters were applied to all non-hydrogen atoms. The hydrogen atoms were generated geometrically. To keep the anisotropic thermal parameters of the disordered trifluoromethyl and ethyl groups of MAF-9 within reasonable limits, ISOR restrictions were used in the refinements. Crystal data were summarized in Table S1.

Description/analysis of the crystal structures used the true C–H bond length of 1.1 Å. The void

ratio was calculated by the SOLV route of PLATON 130220, using the default setting (probe radius of 1.2 Å). The void ratio of MAF-9 containing disordered ethyl groups was calculated as the average value of the two values supposing the material adopts two extreme structures.

PXRD patterns were collected on a Bruker D8 DAVINCI X-ray powder diffractometer with  $CuK\alpha$  radiation in the transmission mode at room temperature. Pawley refinements of PXRD data were performed in the  $2\theta$  range of  $5\text{--}40^\circ$  on unit-cell parameters, zero point and background terms with Pseudo-Voigt profile function and Berar-Baldinozzi asymmetry correction function. All the indexing and refinements were performed by the Reflex plus module of Materials Studio 5.5.

## Computational details

All simulations/calculations were performed using the Materials Studio 5.5 package. All the gas adsorption sites were generated from Grand Canonical Monte Carlo (GCMC) simulations with the fixed pressure task (at 195 K and 1 atm) in the Sorption module. The host frameworks and  $CO_2$  molecules were both regarded as rigid. The simulation box contained one unit cell, and the Metropolis method based on the universal force field (UFF) was used. Mulliken charges calculated from Density Functional Theory (DFT) were adopted for all the atoms of the host frameworks and  $CO_2$  molecules [48], with the grid interval of 0.4 Å. The cutoff radius was chosen as 12.5 Å for the Lennard-Jones potential, and the electrostatic interactions and van der Waals interactions were handled using the Ewald and Atom based summation methods, respectively. All the equilibration steps and production steps were set as  $5 \times 10^6$ .

Before the GCMC simulations, full geometry optimizations were performed according to the literature [21]. The widely used generalized gradient approximation (GGA) with the Perdew–Burke–Ernzerhof (PBE) functional and the double numerical plus d-functions (DND) basis set, as well as the DFT Semicore Pseudopotentials (DSPP) were used. The energy, gradient and displacement convergence criteria were set as  $2 \times 10^{-5}$  Ha,  $4 \times 10^{-3}$  Å and  $5 \times 10^{-3}$  Å, respectively.

## SUPPLEMENTARY DATA

Supplementary data are available at [NSR](https://doi.org/10.1093/nsr/nwab094) online.

## FUNDING

This work was supported by the National Natural Science Foundation of China (21731007 and 21821003) and the Guangdong Pearl River Talents Program (2017BT01C161).

## AUTHOR CONTRIBUTIONS

J.-P.Z. conceived and designed the project. C.W. synthesized compounds and performed most of the experiments and data analyses. D.-D.Z., Y.-W.G., X.-W.Z. and Z.-M.Y. assisted with the experiments and data analyses. D.-D.Z. conducted computation simulations and slide angle measurements. J.-P.Z. and C.W. co-wrote the paper. All authors discussed the results and commented on the manuscript.

**Conflict of interest statement.** None declared.

## REFERENCES

- Yuan S, Feng L and Wang K *et al.* Stable metal–organic frameworks: design, synthesis, and applications. *Adv Mater* 2018; **30**: 1704303.
- Li H, Li L and Lin R-B *et al.* Porous metal-organic frameworks for gas storage and separation: status and challenges. *EnergyChem* 2019; **1**: 100006.
- Wang H and Li J. Microporous metal–organic frameworks for adsorptive separation of C5–C6 alkane isomers. *Acc Chem Res* 2019; **52**: 1968–78.
- Cui X, Chen K and Xing H *et al.* Pore chemistry and size control in hybrid porous materials for acetylene capture from ethylene. *Science* 2016; **353**: 141–4.
- Zhang J-P, Zhou H-L and Zhou D-D *et al.* Controlling flexibility of metal–organic frameworks. *Natl Sci Rev* 2018; **5**: 907–19.
- Chang Z, Yang D-H and Xu J *et al.* Flexible metal–organic frameworks: recent advances and potential applications. *Adv Mater* 2015; **27**: 5432–41.
- Yang H, Trieu TX and Zhao X *et al.* Lock-and-key and shape-memory effects in an unconventional synthetic path to magnesium metal–organic frameworks. *Angew Chem Int Ed* 2019; **58**: 11757–62.
- Krause S, Bon V and Senkovska I *et al.* A pressure-amplifying framework material with negative gas adsorption transitions. *Nature* 2016; **532**: 348–52.
- Shivanna M, Yang Q-Y and Bajpai A *et al.* A dynamic and multi-responsive porous flexible metal–organic material. *Nat Commun* 2018; **9**: 3080.
- Duan J, Zhang Q and Wang S *et al.* Controlled flexibility of porous coordination polymers by shifting the position of the –CH<sub>3</sub> group around coordination sites and their highly efficient gas separation. *Inorg Chem Front* 2018; **5**: 1780–6.
- Mason JA, Oktawiec J and Taylor MK *et al.* Methane storage in flexible metal–organic frameworks with intrinsic thermal management. *Nature* 2015; **527**: 357–61.
- Yang S, Lin X and Lewis W *et al.* A partially interpenetrated metal–organic framework for selective hysteretic sorption of carbon dioxide. *Nat Mater* 2012; **11**: 710–6.
- Xie L-H, Xu M-M and Liu X-M *et al.* Hydrophobic metal–organic frameworks: assessment, construction, and diverse applications. *Adv Sci* 2020; **7**: 1901758.
- Rao KP, Higuchi M and Sumida K *et al.* Design of superhydrophobic porous coordination polymers through the introduction of external surface corrugation by the use of an aromatic hydrocarbon building unit. *Angew Chem Int Ed* 2014; **53**: 8225–30.
- Mukherjee S, Kansara AM and Saha D *et al.* An ultrahydrophobic fluorinated metal–organic framework derived recyclable composite as a promising platform to tackle marine oil spills. *Chem Eur J* 2016; **22**: 10937–43.
- Rao KP, Higuchi M and Suryachandram J *et al.* Temperature-stable compelled composite superhydrophobic porous coordination polymers achieved *via* an unattainable *De novo* synthetic method. *J Am Chem Soc* 2018; **140**: 13786–92.
- He C-T, Jiang L and Ye Z-M *et al.* Exceptional hydrophobicity of a large-pore metal–organic zeolite. *J Am Chem Soc* 2015; **137**: 7217–23.
- Xie L-H, Liu X-M and He T *et al.* Metal–organic frameworks for the capture of trace aromatic volatile organic compounds. *Chem* 2018; **4**: 1911–27.
- Wang JH, Li M and Li D. An exceptionally stable and water-resistant metal–organic framework with hydrophobic nanospaces for extracting aromatic pollutants from water. *Chem Eur J* 2014; **20**: 12004–8.
- Wang C, Huang J and Huang R-K *et al.* Partially fluorinated Cu(I) triazolate frameworks with high hydrophobicity, porosity, and luminescence sensitivity. *Inorg Chem* 2019; **58**: 3944–9.
- Zhou D-D, Chen P and Wang C *et al.* Intermediate-sized molecular sieving of styrene from larger and smaller analogues. *Nat Mater* 2019; **18**: 994–8.
- Moghadam PZ, Ivy JF and Arvapally RK *et al.* Adsorption and molecular siting of CO<sub>2</sub>, water, and other gases in the superhydrophobic, flexible pores of FMOF-1 from experiment and simulation. *Chem Sci* 2017; **8**: 3989–4000.
- Yang C, Kaipa U and Mather QZ *et al.* Fluorous metal–organic frameworks with superior adsorption and hydrophobic properties toward oil spill cleanup and hydrocarbon storage. *J Am Chem Soc* 2011; **133**: 18094–7.
- Chen T-H, Popov I and Zenasni O *et al.* Superhydrophobic perfluorinated metal–organic frameworks. *Chem Commun* 2013; **49**: 6846–8.
- Fritzsche J, Denysenko D and Grzywa M *et al.* CFA-13 – a bifunctional perfluorinated metal–organic framework featuring active Cu(I) and Cu(II) sites. *Dalton Trans* 2017; **46**: 14907–15.
- Fritzsche J, Ettlenger R and Grzywa M *et al.* CFA-15 – a perfluorinated metal–organic framework with linear 1-D CuII-chains containing accessible unsaturated, reactive metal centres. *Dalton Trans* 2019; **48**: 15236–46.
- Yang C, Wang X and Omary MA. Fluorous metal–organic frameworks for high-density gas adsorption. *J Am Chem Soc* 2007; **129**: 15454–5.
- Galli S, Cimino A and Ivy JF *et al.* Fluorous metal–organic frameworks and nonporous coordination polymers as low- $\kappa$ , dielectrics. *Adv Funct Mater* 2019; **29**: 1904707.



29. DeFuria MD, Zeller M and Genna DT. Removal of pharmaceuticals from water via  $\pi$ - $\pi$  stacking interactions in perfluorinated metal-organic frameworks. *Cryst Growth Des* 2016; **16**: 3530-4.
30. D'Amato R, Donnadio A and Carta M *et al.* Water-based synthesis and enhanced CO<sub>2</sub> capture performance of perfluorinated cerium-based metal-organic frameworks with UiO-66 and MIL-140 topology. *ACS Sustain Chem Eng* 2019; **7**: 394-402.
31. Jeon HJ, Matsuda R and Kanoo P *et al.* The densely fluorinated nanospace of a porous coordination polymer composed of perfluorobutyl-functionalized ligands. *Chem Commun* 2014; **50**: 10861-3.
32. Deng H, Grunder S and Cordova KE *et al.* Large-pore apertures in a series of metal-organic frameworks. *Science* 2012; **336**: 1018.
33. Roy S, Suresh VM and Maji TK. Self-cleaning MOF: realization of extreme water repellence in coordination driven self-assembled nanostructures. *Chem Sci* 2016; **7**: 2251-6.
34. Rao KP, Devi YK and Suryachandram J *et al.* A dense I<sup>1</sup>O<sup>3</sup> hybrid superhydrophobic network, Pb(H-BTMB), exhibits selectivity toward CO<sub>2</sub> gas sorption. *Inorg Chem* 2017; **56**: 11184-9.
35. Yang C, Wang X and Omary MA. Crystallographic observation of dynamic gas adsorption sites and thermal expansion in a breathable fluorinated metal-organic framework. *Angew Chem Int Ed* 2009; **48**: 2500-5.
36. Abdul-Ghani MM and Tipping AE. Unsaturated nitrogen compounds containing fluorine. Part 16. The synthesis of 3,5-bis(trifluoromethyl)-1*H*-1,2,4-triazole and some 4-substituted derivatives from 2,5-dichloro-1,1,1,6,6,6-hexafluoro-3,4-diazahexa-2,4-diene. *J Fluorine Chem* 1995; **72**: 95-106.
37. Zhang J-P, Zhang Y-B and Lin J-B *et al.* Metal azolate frameworks: from crystal engineering to functional materials. *Chem Rev* 2012; **112**: 1001-33.
38. Zhang J-P and Chen X-M. Exceptional framework flexibility and sorption behavior of a multifunctional porous cuprous triazolate framework. *J Am Chem Soc* 2008; **130**: 6010-7.
39. Liu S-Y, Qi X-L and Lin R-B *et al.* Porous Cu(I) triazolate framework and derived hybrid membrane with exceptionally high sensing efficiency for gaseous oxygen. *Adv Funct Mater* 2014; **24**: 5866-72.
40. Xue H, Twamley B and Shreeve JM. The first 1-alkyl-3-perfluoroalkyl-4,5-dimethyl-1,2,4-triazolium salts. *J Org Chem* 2004; **69**: 1397-400.
41. Yang G, Zhang P-P and Liu L-L *et al.* 3D binary silver(I) 1,2,4-triazolates: syntheses, structures and topologies. *CrystEngComm* 2009; **11**: 663-70.
42. Yang X, Wang Y and Zhou H-L *et al.* Guest-containing supramolecular isomers of silver(I) 3,5-dialkyl-1,2,4-triazolates: syntheses, structures, and structural transformation behaviours. *CrystEngComm* 2015; **17**: 8843-9.
43. Zhai Q-G, Hu M-C and Li S-N *et al.* Synthesis, structure and blue luminescent properties of a new silver(I) triazolate coordination polymer with 8<sup>2</sup>10-a topology. *Inorg Chim Acta* 2009; **362**: 1355-7.
44. Yang G, Duan P-C and Shi K-G *et al.* Relaying isomerism from ligands to metal complexes: synthesis and structures of four isomeric binary silver(I) 3,5-dibutyl-1,2,4-triazolates. *Cryst Growth Des* 2012; **12**: 1882-9.
45. Zhang W-H, Wang Y-H and Li Y-W *et al.* Synthesis and structures of silver(I) and copper(I) 3,5-dipentyl-1,2,4-triazolates. *J Cluster Sci* 2012; **23**: 411-20.
46. Zhang J-P and Chen X-M. Optimized acetylene/carbon dioxide sorption in a dynamic porous crystal. *J Am Chem Soc* 2009; **131**: 5516-21.
47. Sing KSW, Everett DH and Haul RAW *et al.* Reporting physisorption data for gas/solid systems with special reference to the determination of surface area and porosity. *Pure Appl Chem* 1985; **57**: 603-19.
48. Zhou D-D, He C-T and Liao P-Q *et al.* A flexible porous Cu(II) bis-imidazolate framework with ultrahigh concentration of active sites for efficient and recyclable CO<sub>2</sub> capture. *Chem Commun* 2013; **49**: 11728-30.